Melting Behavior of Poly(trimethylene terephthalate)

WEI-TSUNG CHUNG, WEI-JUN YEH, PO-DA HONG

Department of Fiber and Polymer Engineering, National Taiwan University of Science and Technology, Taipei 10607, Taiwan

Received 20 February 2001; accepted 8 July 2001

ABSTRACT: In this study, the melting behavior of isothermally crystallized polytrimethylene terephthalate (PTT) was investigated. Multiple melting behaviors in DSC heating trace were found because two populations of lamellar stacks were formed during primary crystallization and the recrystallization at heating process, respectively. This fact could be also confirmed from the result of optical microscopy observation. The Hoffman–Weeks equation was applied to obtain equilibrium melting temperature (T_m^0). The T_m^0 value of PTT is about 525 K, which is 10 K higher than that reported. Combining the enthalpy of fusion from the DSC result and the degree of crystallinity from WAXD result, the value of the equilibrium-melting enthalpy ΔH_f^0 was deduced to be approximately 28.8 kJ mol^{-1}. © 2002 John Wiley & Sons, Inc. J Appl Polym Sci 83: 2426–2433, 2002

Key words: poly(trimethylene terephthalate); melting behavior; Hoffman–Weeks equation

INTRODUCTION

Poly(trimethylene terephthalate) (PTT) was recently introduced as a commercial polymer, joining the polyester family with others such as poly(ethylene terephthalate) (PET) and poly(butylene terephthalate) (PBT). The synthetic method of PTT was first reported by Whinfield and Dickson.[1] The products are difficult to commercialize because of the lack of an economical source of trimethylene glycol, also called 1,3-propandiol monomer. Nevertheless, the synthesis of PTT is now available in industrial quantities for use in fiber and engineering thermoplastic applications developed by Shell Chemical Co.[2–6] Because PTT is a relatively new material, little structural information is reported in the literature. Some studies[7,8] have reported that the unit cell of PTT crystal is triclinic and each cell contains two monomers of one polymer chain each, of which methylene bonds are in the *gauche* conformation (i.e., 3 GT conformation).

Owing to the methylene groups in the main chain, the flexibility of PTT chain should be higher than that of PET chain. This may give rise to the fast crystallization of PTT compared with that of PET. Recently, Pyda et al.[9] reported some thermal parameters such as heat capacity, equilibrium temperature, and enthalpy of PTT in their article. From their results, we were very interested in the value of the equilibrium temperature T_m^0 (510 K) that they used to calculate the heat capacity, because this value is only 9 K higher than the melting temperature T_m (501 K) of the sample crystallized from the partial-quenched state (the data shown in Fig. 4 of their article). Generally, the difference between T_m^0 and T_m values for flexible polymers is above 20 K, if the crystallization does not occur at extremely high temperatures to form a very large size lamellar thickness. Thus, the T_m^0 value may need to be reconfirmed through thermal analyses.

Correspondence to: P.-D. Hong (phong@hp730.tx.ntust.edu.tw).

Journal of Applied Polymer Science, Vol. 83, 2426–2433 (2002)
© 2002 John Wiley & Sons, Inc.
DOI 10.1002/app.10206

The melting behavior of isothermally crystallized polymers was one of the most important studies in the field of polymer engineering. The multiple melting behaviors identified by the thermal effect leading to recrystallization or reorganization processes are generally carried out during DSC scanning and the secondary crystallization in the Avrami curve at the nonlinear stage. Recently, many studies[10–13] reported that there may be dual populations of lamellar stacks formed from the recrystallization, resulting in multiple melting behaviors. However, there are still many arguments in the proposed models for a controversy over the multiple melting behaviors. Generally, terephalate polyesters often exhibit multiple melting peaks in the DSC results; however, up to now there is no information about the melting behavior for PTT.

In this study, the multiple melting behavior of PTT is discussed to clarify the relation between the crystallization and melting behaviors. Then, some equilibrium values of thermal parameters such as the equilibrium melting temperature, the equilibrium melting enthalpy, and entropy were calculated compared with those reported in the literature.

EXPERIMENTAL

Materials

PTT was kindly supplied by Industrial Technology Research Institute (ITRI), Hsin-Chu, Taiwan, China. The PTT used in this work was obtained by the direct esterification of 1.3-propanediol (PDO) with terephthalic acid (TPA) in the melt phase with tetraisopropyl titanate as the catalyst. The intrinsic viscosity of the PTT obtained from a phenol/tetrachloroethane (60/40)-mixed solution at 298 K is ~ 0.84 mL/g. According to published results reported by Chuah et al.,[14] the relationship between number-average molecular weight and intrinsic viscosity of the PTT is $[\eta]_{\text{phenol/tetrachloroethane}} = 5.36M^{0.69}$. Therefore, the number-average molecular weight of ~ 43,000 can be estimated. All specimens were dried at 363 K for 3 h under vacuuming before any new thermal treatment or experimental characterizations.

Measurements

The measurements of differential scanning calorimeter (DSC) were carried out by using a DuPont 2000 Thermal Analyzer. Typically, the sample was first melted at 553 K for 5 min to make an isothermal crystallization and then liquid nitrogen was used to quickly cool (ca. 100 K/min) the sample to ambient crystallization temperature. The subsequent heating curves at a heating rate of 10 K/min were recorded for various crystallization times. All measurements were performed at a dry nitrogen atmosphere. The instrument was calibrated in both the temperature and the melting enthalpy with a standard sample of indium. The heat of fusion of indium (28.45 J g^{-1}) was used to calibrate the thermal response of the calorimeter. To avoid an uneven thermal conduction of the samples, which may cause different amounts of broadening and shifting of the peak positions, the aluminum pans were always filled with the same quantity of specimen, about 10 ± 1 mg.

The radial growth of PTT spherulite was observed by using polarized light microscopy (PLM) (Leica Laborlux 12 Pols) with a hot stage (Linkman CI93). The specimens were first melted at 553 K for 5 min and then rapidly cooled to the selected crystallization temperature with liquid nitrogen. When the crystallization temperature was reached, the radial growth of the spherulite was recorded with a camera.

The wide-angle X-ray diffraction (WAXD) intensity curves of the samples were measured by using a Rigaku D/max diffractometer with a graphite-monochromatized CuKα radiation working at 40 KV and 100 mA at a scanning rate of 1°/min. The amorphous PTT was prepared from quick quenching of melted PTT. This sample is indeed amorphous from the results of WAXD and DSC, as shown in Figure 1. In DSC heating trace, the total exothermic enthalpy of crystallization is almost the same with the melting enthalpy. On the other hand, the WAXD profile only exhibited an amorphous scattering pattern without any crystalline diffraction.

RESULTS AND DISCUSSION

Figure 2 shows the DSC heating traces where the isothermal crystallization of PTT has completely taken place at various crystallization temperatures, T_c. The endothermic peaks labeled I, II, and III change their position with T_c. At $T_c < 463$ K, only two melting peaks were observed (i.e., the highest temperature peak I at ca. 501–503 K and low temperature peak II at around 490 K). For the sample crystallized at $T_c = 463$ K, a small peak III appeared. Meanwhile, at $T_c > 473$ K, peak I suddenly disappeared and then peak III and peak II gradu-

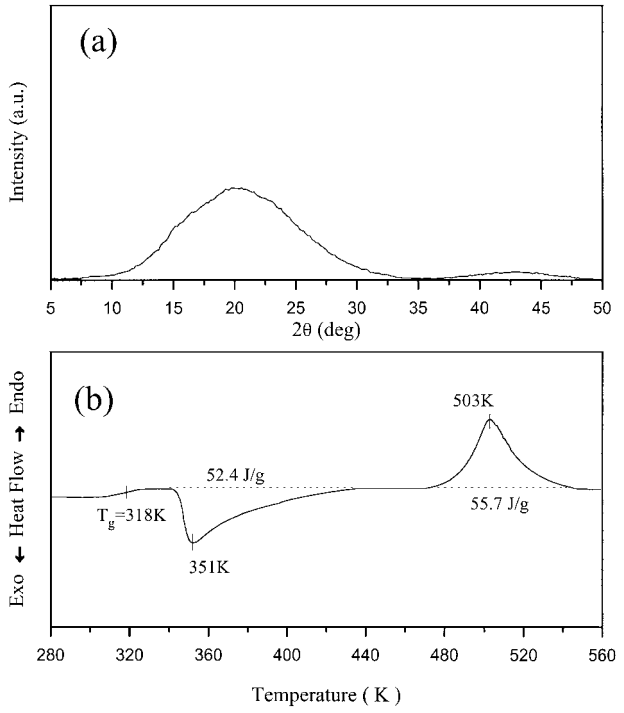

Figure 1 WAXD pattern (a) and DSC trace (b) for completely amorphous PTT.

ally developed with T_c. The only single peak is observed for sample crystallized at T_c = 488 K. However, the multiple melting behaviors were reported in many polymers.[10–13,15–20] There still exists some disagreement concerning the origins of multiple

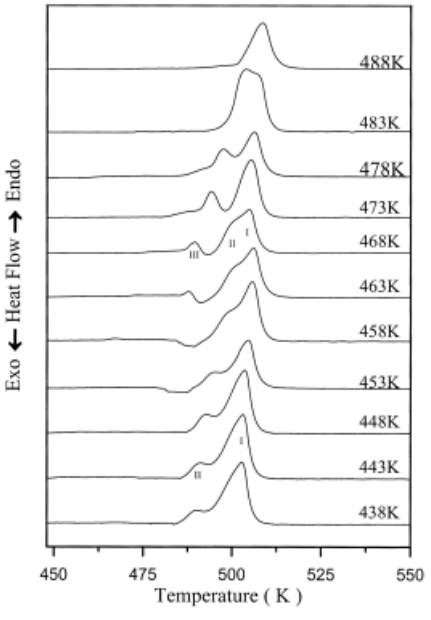

Figure 2 DSC traces of PTT at various T_c (heating rate, 10 K/min).

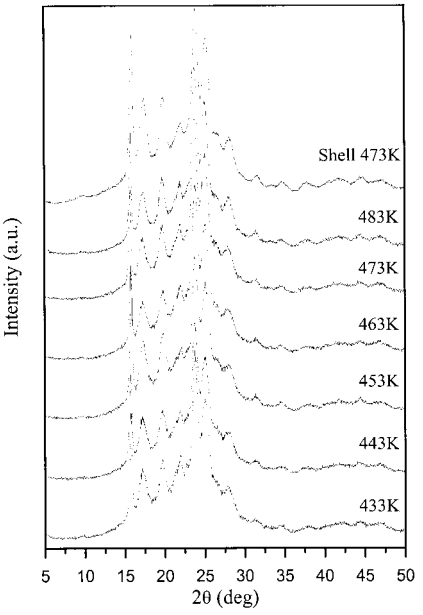

Figure 3 Evolution of WAXD pattern as function of T_c.

melting behaviors. Generally, the multiple melting behaviors could be considered to be related to the formation of various crystal structures or the dual lamellar stack during primary crystallization, the effect of secondary crystallization and the recrystallization or reorganization during DSC heating trace. The different crystal structures were formed when the polymer exhibits polymorphism of crystal structure such as Nylon-6,6[21] and it-PP.[22] The secondary crystallization can usually be identified by the deviation of an Avrami plot at the nonlinear stage where the spherulites may impinge with each other and their growth may either be related to subsidiary lamellae or to thickening of lamellae. Another reason is the reorganization of metastable crystals during heating, which may result in only crystal perfection and/or crystal thickening concerning the heating rate. Under these backgrounds mentioned above, we suggest several experimental methods for obtaining a clear understanding of multiple melting behaviors for PTT.

The WAXD patterns corresponding to the isothermally crystallized samples are shown in Figure 3. There is no shift of the position (2θ) in the diffraction peaks, indicating that the crystal unit cell of PTT does not change with crystallization temperature. Therefore, the formation of the polymorphism of crystal structure is not the origin of multiple melting behaviors for PTT. Simultaneously, Figure 3 also shows the same crystal structure for PTTs of the present study and Shell Co.

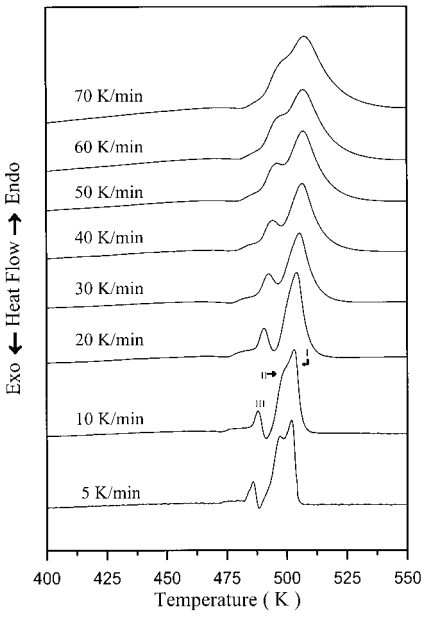

Figure 4 DSC heating traces of 468 K crystallized PTT at various heating rates.

Figure 4 shows the DSC heating trace as a function of the heating rate for PTT after isothermal crystallization at 468 K. The triple melting peaks are still found for the heating rate of 10 and 5 K/min. Meanwhile, it only shows two melting peaks beyond the heating rate of 30 K/min. As the heating rate is further increased, only one broader peak could be found. Summarizing, in the melting peaks for the samples with various heating rates at T_c = 468 K, three melting peaks could be detected (i.e., peak III at ca. 486 K, peak II at ca. 500 K, and peak I at around 505 K). Peak II overlaps with peak I to produce one broader peak at a heating rate of 30 K/min, leading to dual melting peaks. There is a small exotherm at $\sim$ 408 K in Figures 2 and 4. We do not agree that the recrystallization can take place at such a high temperature during the heating process when the isothermal crystallization was completed. This peak III may be related to a slight ordering exotherm that causes partly premelting of crystals to give rise to less metastability due to thermal fluctuation. In fact, the faster heating rate may shift the peak temperature because of the superheating due to the effect of thermal lag. As the heating rate is further increased, three melting peaks shift significantly to much higher temperatures. For this reason, peak II was not related to the subsequent recrystallization or reorganization during heating process.

We still doubted whether the secondary crystallization and recrystallization (or reorganization) cause the multiple melting behaviors. However, this is not so easy to judge from the results in Figure 4 because the faster heating rate would lead the melting peak shift to a higher temperature and the recrystallization or secondary crystallization was not discriminated from the DSC traces. Based upon Avrami theory, it generally defines the linear stage as the primary crystallization and the nonlinear stage as the secondary crystallization. Therefore, we set a limit of the isothermal crystallization at linear stage (i.e., the sample was quickly quenched by liquid nitrogen to inhibit the secondary crystallization). To measure the original melting of the primary crystallization, the higher heating rate is necessary to prevent the effect of recrystallization during the heating process. The heating traces of the samples crystallized at T_c = 468 K with various heating rates are shown in Figure 5. The peak-fitting procedure was used to separate three melting peaks. In Figure 5, a relatively clear curve of the triple melting peaks was found for the sample at the heating rate of 10 K/min. Owing to the fast crystallization, it does not have enough time to restrain the recrystallization. A slight recrystallization peak depending on the heating rate was found in the temperature range from 333 to 383 K and its exothermic enthalpy corresponds well to the endothermic enthalpy of peak III. For this reason, peak III was considered attributed to the recrystallization during the heating process. However, peak I and II, found in Figure 5, should be concerned with the primary crystallization. This result is in agreement with that in Figure 4, which leads us to consider that two populations of lamellar stack were formed during the primary crystallization, resulting in the dual melting be-

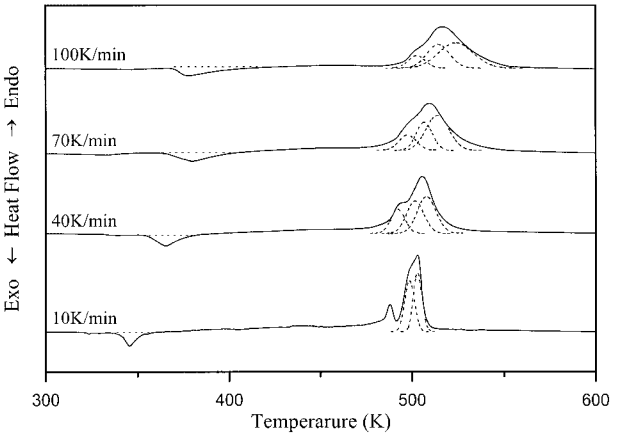

Figure 5 DSC heating traces as a function of heating rate for 468 K crystallized PTT at Avrami linear stage.

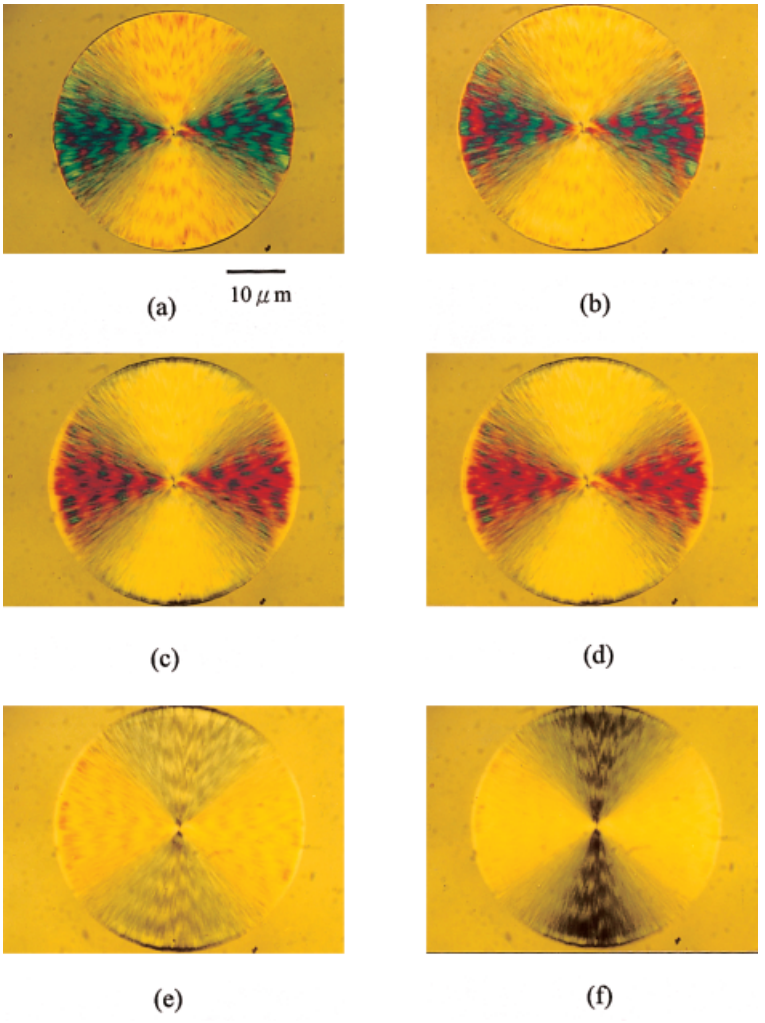

Figure 6 The heating traces of PLM photographs of insertion of the λ/4 compensator for 468 K crystallized PTT at Avrami linear stage: (a) 468 K, (b) 495 K, (c) 497 K, (d) 500 K, (e) 503 K, (f) 505 K.

havior (peaks I and II). The two populations of lamellar stack may be associated with the lamellar-branching effect for the growth of the spherulites.[23–25]

Additionally, we also provide other evidence from optical microscopy, which was inserted into the λ/4 compensator for spherulite of PTT, as shown in Figure 6. The sample was isothermally crystallized at 468 K, as the crystallization time is kept within the Avrami linear region and then subsequently heated at a heat rate of 10 K/min. Actually, after insertion of the λ/4 compensator, the Maltese cross extinction pattern becomes unapparent and displays gray, and it is divided into four quadrants of cross. Based on the optical theory, the differential velocity of propagation of both rays causes a phase difference Γ, which depends both on the magnitude of the effective birefringence Δn and on the thickness d of the object[26–29]:

$$\Gamma = d \times \Delta n \tag{1}$$

Depending on the Γ value in the specimen, a specific interference color will appear. If we assume that the birefringence remains constant in all samples at the same thermal history, the increase in phase difference may be considered due mainly to the change in thickness.[27,30]

To account for the relation between the melting temperature and the lamellar thickness, the Thomson–Gibbs equation[31] is generally used

$$T_m = T_m^0\left[1 - \frac{2\sigma_e}{\Delta H_f^0 l}\right] \tag{2}$$

where T_m^0 is the equilibrium melting temperature, σ_e is the surface-free energy, ΔH_f^0 is the

equilibrium melting enthalpy, and l is the lamellar thickness, respectively. In eq. (2), if the σ_e value is assumed constant, the melting temperature will be directly proportion to lamellae thickness, l. In Figure 6, even though for publication purposes the micrographs shown are black and white, the true sequence of the formation of PTT spherulite was characterized by sequential development of the interference colors when there is an increase of phase difference by changing the lamellar thickness at constant birefringence. At temperatures below 495 K, the interference colors in the first and third diametrically opposed quadrants of the cross are orange and those in the second and fourth diametrically opposed quadrants are green [Figs. 6(a) and (b)]. Meanwhile, the temperature was heated to 497–500 K, the interference colors in the first and third quadrants of the cross were still orange, but in the second and fourth quadrants of the cross become red [Figs. 6(c) and (d)]. Finally, the interference colors in the first and third quadrants become black and in the second and fourth quadrants the interference colors become orange [Figs. 6(e) and (f)]. A combination of the results in Figures 5 and 6 is in agreement with the discussions in eqs. (1) and (2) (i.e., two populations of lamellar stack related peaks I and II can be deduced from the change in the interference colors with temperature). It may also imply that the thickest mother lamellae (peak I) were first formed and then the branched lamellae (peak II) infill spherulites during primary crystallization.[27,32] This branched effect may be analogously reported by Medellín-Rodríguez et al.[27] On the other hand, less variety of color was observed by increasing the crystallization temperature, indicating that the lamellar thickness became more homogeneous at higher T_c. This result corresponds well to that of Figure 2, where the triple melting peaks evolve into one broader peak with increasing crystallization temperature.

Determination of Equilibrium Melting Temperature

The equilibrium melting point T_m^0 denotes the melting temperature of the infinite crystal with extended chain conformation and the greatest degree of perfection. Generally, the T_m^0 value could be determined by using the Hoffman–Weeks equation,[23–25]

$$T_m = (1/\gamma)T_c + (1 - 1/\gamma)T_m^0 \qquad (3)$$

where T_m is the observed melting temperature, T_c is the crystallization temperature, and $\gamma = l/l^*$ is the ratio of the lamellar thickness l to the thickness l^* of the critical nuclei at T_c, respectively. The T_m^0 value and the lamellar thickening factor γ could be easily obtained from the intersection at the $T_m = T_c$ line and the slope, respectively, from the classic Hoffman–Weeks plot shown in Figure 7. The melting temperatures related to various lamellar sizes could finally extrapolate to the $T_m = T_c$ line for obtaining the T_m^0 value of ~ 525 K. The γ values are 3.26, 2.28, and 1.66 from the calculations of the triple melting peaks, respectively. It should be mentioned that our T_m^0 value of 525 K for PTT is higher that that (T_m^0 = 510 K) reported in the literature.[2,9] The T_m^0 value of 510 K may be underestimated for PTT with the melting temperature of about 503–505 K because PTT chain is not so rigid to easily form the extended chain crystallite under general crystallization from the partial quenched state.

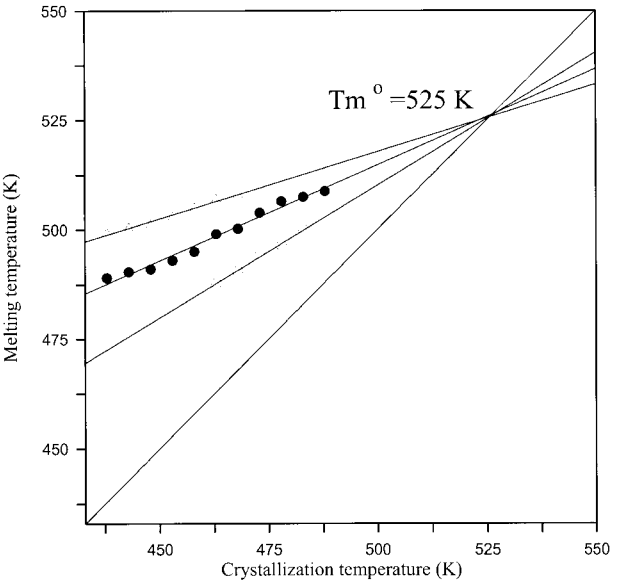

Figure 7 Hoffman–Weeks plot for the PTT. Filled circle, hollowed circle, and triangle indicate the melting peaks I, II, and III, respectively.

Determination of Equilibrium Melting Enthalpy

The equilibrium melting enthalpy for the 100% crystalline sample was estimated by using a combination of DSC and WAXD analyses. In analyzing WAXD data, the background scattering was subtracted from total intensity curve. The value of the crystalline fraction W_c is then obtained from[33–35]:

$$W_c = \frac{I_c}{I_c + kI_a} \qquad (4)$$

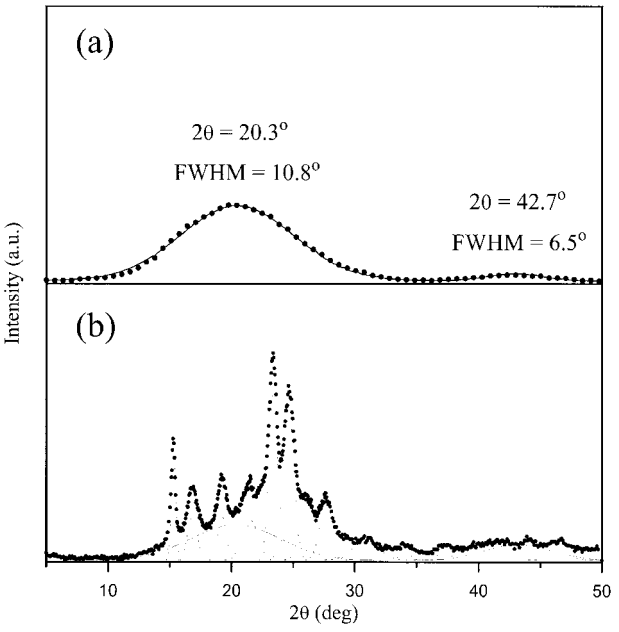

Figure 8 Profile analysis of WAXD intensity curve: (a) the scattering profile for amorphous PTT; (b) the profile analysis for the sample crystallized at T_c = 488 K for 3 h.

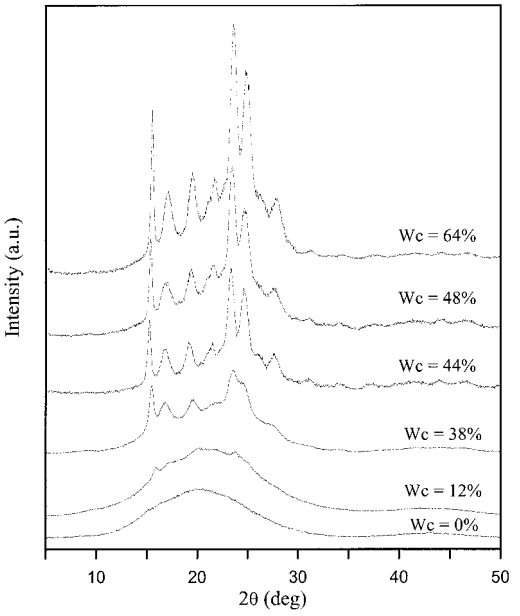

Figure 9 The crystallinity of PTT crystallized at T_c = 488 K for various crystallization times, t = 0, 0.5, 1, 3, 7, and 12 h, respectively.

where I_a is the intensity of amorphous scattering, I_c is the intensity of the crystalline diffraction, and k is the correct factor, respectively. This procedure involves the separation of X-ray scattering intensities into amorphous and crystalline components. To separate the crystalline fraction from the total intensity, the Gaussian function was applied to fit each crystalline diffraction peak. The intensity curve of the completely amorphous sample shown in Figure 1(a) was used for the peak separation. We should first assume that the positions (2θ) and FWHM (full width at half-maximum) of the amorphous scattering peak must be constant (i.e., the structure of amorphous phase has no change with various crystallization conditions).

Figure 8(a) shows the amorphous scattering peaks, which the FWHM was fixed at 10.8° and 6.5° at the constant 2θ of 20.3° and 42.7°, respectively. The pattern of peak separation is shown in Figure 8(b). The degree of crystallinity was estimated by using this procedure. Figure 9 shows a series of WAXD curves for the samples with various degrees of crystallinity. The corresponding melting enthalpy of the sample was obtained from DSC measurement. Combining WAXD and DSC results, Figure 10 shows the relation between the melting enthalpy and crystallinity. A linear relationship was well obtained, and then the extrapolation to 100% crystalline sample could give a value of 28.8 kJ mol^{-1} for equilibrium melting enthalpy ΔH_f^0 of PTT. This value is in good agreement with that reported by Pyda et al.[9] The equilibrium melting entropy ΔS_f^0 from the calculation in $T_m^0 = \Delta H_f^0/\Delta S_f^0$ is $\sim$ 54.8 JK^{-1} mol^{-1}.

CONCLUSION

In this work, the melting behavior for isothermally crystallized PTTs was investigated. The tri-

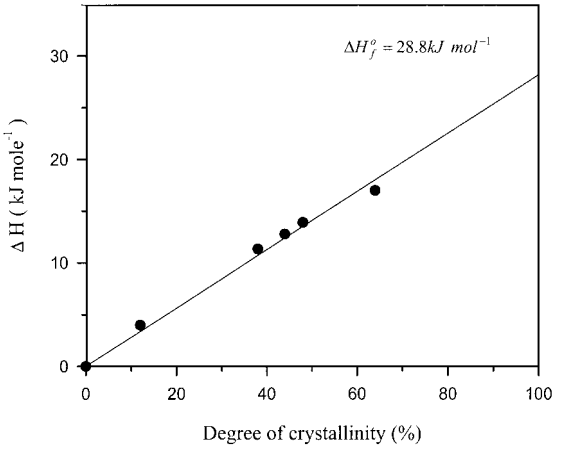

Figure 10 The plot of the heat of fusion versus the degree of crystallinity for PTT.

ple endotherms were found for PTT at various conditions of crystallization. Peaks I and II with higher melting temperatures were considered attributed to primary crystallization. On the other hand, peak III was related to the recrystallization. These melting peaks evolve into one peak at high-crystallization temperature, because the order of lamellae structure was increased due to a lower degree of undercooling. Presumably, the branched effect may take place in the primary crystallization to bring about two populations of lamellar stack. The equilibrium melting temperature of PTT T_m^0 was determined from the Hoffman–Weeks equation, being 525 K. Combining the heat of fusion from DSC with the crystallinity from WAXD, the equilibrium enthalpy of PTT ΔH_f^0 was deduced to be 28.8 kJ mol^{-1}.

REFERENCES

1. Brit. Pat. 578,079, 1941; U.S. Pat. 2 465,319, 1949.
2. Grebowicz, J.; Chuah, H. H. Progress Report, Shell Chemical Co., 1996.
3. Chuah, H. H. Chem Fiber Int 1996, 46, 424.
4. Brown, H. S.; Chuah, H. H. Chem Fiber Int 1997, 47, 72.
5. Shell Chemicals' online literature www address: http://www.shellchemical.com/CMM/WEB/Globchem.NSF/Literature/SC:PTT2.
6. Dangayach, K.; Chuah, H.; Gergen, W.; Dalton, P.; Smith, F. Plastics—Saving Planet Earth; 55th ANTEC Proc., 1997, 2907.
7. Poulin-Dandurand, S.; Perez, S.; Revol, J.; Brisse, F. Polymer 1979, 20, 419.
8. Desborough, I. J.; Hall, I. H.; Neisser, J. Z. Polymer 1979, 20, 545.
9. Pyda, M.; Boller, A.; Grebowicz, J.; Chuah, H.; Lebedev, B. V.; Wunderlich, B. J Polym Sci, Part B: Polym Phys 1998, 36, 2499.
10. Hsiao, B. S.; Sauer, B. B.; Verma, R. K.; Zachmann, H.; Seifert, S.; Chu, B.; Harney, P. Macromolecules 1995, 28, 6931.
11. Verma, R.; Marand, H.; Hsiao, B. Macromolecules 1996, 29, 7767.
12. Hsiao, B. S.; Wang, Z. G.; Yeh, F.; Gao, Y.; Sheth, K. C. Polymer 1999, 40, 3515.
13. Wang, Z. G.; Hsiao, B. S.; Sauer, B. B.; Kampert, W. G. Polymer 1999, 40, 4615.
14. Chuah, H. H.; Lin-Vien, D.; Soni, U. Polymer to appear.
15. Wunderlich, B.; Macromolecular Physics, Vol. 3; Academic Press: New York, 1976.
16. Cheng, S. Z. D.; Zhang, A.; Barley, J. S.; Chen, J.; Habenschuss, A.; Zschack, P. R. Macromolecules 1991, 24, 3937.
17. Medellin-Rodriguez, F. J.; Phillips, P. J. Macromolecules 1995, 28, 7744.
18. Groeninckx, G.; Reynaers, H.; Berghmans, H.; Smets, G. J Polym Sci, Polym Phys Ed 1980, 18, 1311.
19. Lee, Y.; Porter, R. S. Macromolecules 1987, 20, 1336.
20. Kim, H. G.; Robertson, R. E. J Polym Sci, Part B: Polym Phys 1998, 36, 1757.
21. Colclough, M. L.; Baker, R. J Mater Sci 1978, 13, 2531.
22. Mezghani, K.; Phillips, P. Polymer 1998, 39, 3375.
23. Hoffman, J. D.; Week, J. J. J Chem Phys 1962, 37, 1723.
24. Fischer, E. W. Z Naturforsch, A: Phys Sci 1957, 12, 753.
25. Hoffman, J. D.; Davis, G. T.; Lauritzen, J. I., Jr. in Treatise on Solid State Chemistry, Vol. 3; Hannay, N. B., Ed.; Plenum Press: New York, 1976; Chap ter 7.
26. Stoiber, R. E.; Morse, S. A. Crystal Identification with the Polarizing Microscope; Chapman & Hall: New York, 1994.
27. Medellín-Rodríguez, F. J.; Phillips, P. J.; Lin, J. S. Macromolecules 1996, 29, 7491.
28. Padden, F. J.; Keith, H. D. J Appl Phys 1959, 30, 1479.
29. Li, L. S.; Geil, P. H. Polymer 1991, 32, 374.
30. Medellin-Rodriguez, F. J.; Phillips, P. J.; Lin, J. S.; Campos, R. J Polym Sci, Part B: Polym Phys 1997, 35, 1757.
31. Wunderlich, B. Macromolecular Physics; Academic: New York, 1980; Vol. 3, Chapter 8.
32. McCrone, W. C. Polarized Light Microscopy; Ann Arbor Sci. Publishers: Ann Arbor, MI, 1974; Chapter 9.
33. Alexander, L. E. X-ray Diffraction Methods in Polymer Science; Wiley-Interscience: New York, 1969; Chapter 3.
34. Murthy, N. S.; Minor, H. Polymer 1990, 31, 996.
35. Vonk, C. G. J Appl Crystallog 1973, 6, 148.